Journal of Rock Mechanics and Geotechnical Engineering 11 (2019) 325–336

Contents lists available at ScienceDirect

Journal of Rock Mechanics and Geotechnical Engineering

journal homepage: www.rockgeotech.org

Full Length Article

A new framework for evaluation of rock fragmentation in open pit mines

Mohammad Babaeian*, Mohammad Ataei, Farhang Sereshki, Farzad Sotoudeh, Sadjad Mohammadi

Faculty of Mining Engineering, Petroleum and Geophysics, Shahrood University of Technology, Shahrood, Iran

ARTICLE INFO

Article history:
Received 7 May 2018
Received in revised form
29 October 2018
Accepted 5 November 2018
Available online 31 December 2018

Keywords:
Rock fragmentation
Image analysis
Open pit mine
Split-desktop software package
Decision-making trial and evaluation laboratory (DEMATEL) technique

ABSTRACT

The main purpose of blasting in open pit mines is to produce the feed for crushing stage with the optimum dimensions from in situ rocks. The size distribution of muck pile indicates the efficiency of blasting pattern to reach the required optimum sizes. Nevertheless, there is no mature model to predict fragmentation distribution to date that can be used in various open pit mines. Therefore, a new framework to evaluate and predict fragmentation distribution is presented based on the image analysis approach. For this purpose, the data collected from Jajarm bauxite mine in Iran were used as the sources in this study. The image analysis process was performed by Split-Desktop software to find out fragmentation distribution, uniformity index and average size of the fragmented rocks. Then, two different approaches including the multivariate regression method and the decision-making trial and evaluation laboratory (DEMATEL) technique were incorporated to develop new models of the uniformity index and the average size to improve the Rosin-Rammler function. The performances of the proposed models were evaluated in four blasting operation sites. The results obtained indicate that the regression model possesses a better performance in prediction of the uniformity index and the average size and subsequently the fragmentation distribution in comparison with DEMATEL and conventional Rosin-Rammler models.

1. Introduction

Drilling and blasting in open pit mines are the crucial stages as the economy of mining industry generally relies on the optimum design of pattern to reach an appropriate fragmentation. The blasting process, in which the optimal fragmentation and desirable displacement are the main goals, should be carefully considered to address two important issues: reduction of mining costs and increase in production efficiency (Kanchibotla et al., 1998; Michaux and Djordjevic, 2005; Monjezi et al., 2008, 2009). The obtained fragmentation size has a significant influence on downstream operations such as hauling system and secondary crushing that have been extensively studied by numerous researchers (Scott and McKee, 1994; Smith et al., 1994; Kojovic et al., 1995; Nielsen and Kristiansen, 1995). Therefore, evaluation and prediction of rock fragmentation can be the primary and vital step of blasting optimization.

Various methods have been proposed to predict rock fragmentation including uncontrollable methods based on physical and mechanical properties of rocks and controllable methods dependent on design factors such as determination of size distribution and fragmented rocks prediction (Singh and Narendrula, 2009). The controllable methods can be divided into direct and indirect methods, as shown in Fig. 1. In direct methods, measuring the amount of fragmentation is carried out by sieve analysis. Although the accuracy of this method is very high, the high cost and time-consumption are the main drawbacks of this method (Sudhakar et al., 2006). On the other hand, indirect methods including visual, empirical and image analysis techniques provide a trade-off between the accuracy of the test and the amount of time and cost. In visual methods, the distribution of fragmented rocks can be determined with a lower accuracy. In empirical methods, the size distribution of the fragmented rocks is predicted based on various formulae. Although determination of the rock's characterizations and geometries is not accessible through these methods, they are among the most effective and fastest ways to achieve rock mass fragmentation (Lopez and Lopez, 1995; Thornton et al., 2001; Chakraborty et al., 2004; Siddiqui et al., 2009). In image analysis method, the size distribution of fragmented rocks can be determined precisely using the captured images after blasting

* Corresponding author.
E-mail address: Babaeian.sme@gmail.com (M. Babaeian).
Peer review under responsibility of Institute of Rock and Soil Mechanics, Chinese Academy of Sciences.

https://doi.org/10.1016/j.jrmge.2018.11.006

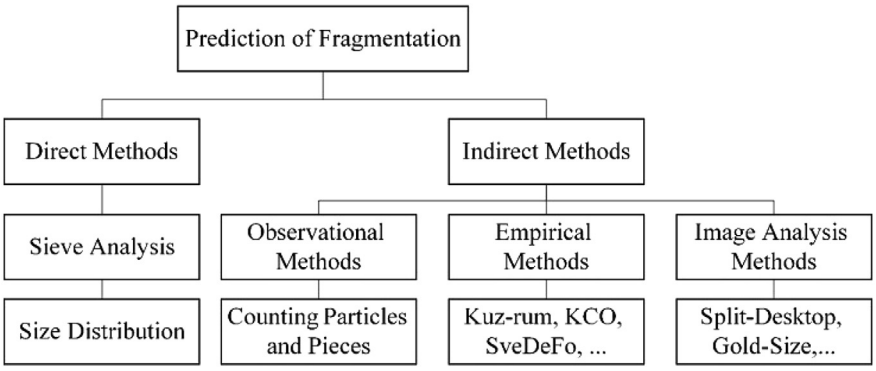

Fig. 1. Main steps of rock fragmentation prediction (modified from Djordjevic, 1998).

operations. The most common software packages for this method are Gold-Size, Split-Desktop, and WipFrag.

Rock fragmentation is a complex dynamic process relating to the interaction between rock mass and explosives. For this reason, a mature model has not yet been developed to meet all mining conditions and geological features (Siddiqui et al., 2009). In order to overcome this drawback, the main goal of this paper is to provide a new framework to evaluate and predict rock fragmentation based on the image analysis utilizing actual data of blasted muck pile. The Jajarm bauxite mine was considered as a case study. In the first step, the interpretation of distribution functions is proposed to identify which function matches with the size distribution. Then, two different approaches were used in order to predict the distribution function variables including the uniformity index and the average size. In the first one, statistical relationships were developed via multivariate regression method. The empirical relationships between the uniformity index, the average size and the introduced indices were proposed using the decision-making trial and evaluation laboratory (DEMATEL) technique in the second approach. Finally, the results of the size distribution diagrams as well as the two modified models were compared and a comprehensive model was proposed according to the existing circumstances to predict the exact fragmentation by blasting.

2. Evaluation of rock fragmentation

There are several methods for assessment and prediction of fragmented rock distribution. Image analysis technique has been widely used due to its high capability of visually processing and providing an appropriate alternative for low-accuracy methods (Hunter et al., 1990). Over the last decades, various image analysis software packages such as Split-Online, Split-desktop, Gold-Size and Wip-Frag have been developed, and their applications to mining industry and mineral processing have been reported. The main advantage of these software packages are integration and lack of disruptions (Sudhakar et al., 2006).

In addition, various functions are available to predict rock fragmentation, such as Rosin-Rammler and Swebrec functions, which are the most widely used methods with respect to uniformity index and mean fragmentation size. The Rosin-Rammler function is presented by Rosin and Rammler (1933) as follows:

$$R(X) = 1 - \exp\left[-\left(\frac{X}{X_c}\right)^n\right] \tag{1}$$

where $R(x)$ is the proportion of passing fragments by the sieve with dimension of X (cm), X_c is the sieve characteristic (the size of fragments which 63.2% will pass through the sieve), and n is the uniformity index. For $R(X) = 0.5$ (i.e. 50% of fragments passing by the sieve), the value of X_c can be measured as follows:

$$X_c = \frac{X}{0.693^{1/n}} \tag{2}$$

Another empirical equation was developed by Swebrec (Ouchterlony, 2005a, b) as follows:

$$P(X) = \left\{1 + \left[\frac{\ln(X_{max}/X)}{\ln(X_{max}/X_{50})}\right]^b\right\}^{-1} \tag{3}$$

where X_{max} is the upper limit of fragmented rocks (burden or spacing of holes); X_{50} is the size of 50% fragments passing through the sieve; and b is an especial index like uniformity index in Kuz-Ram model, which can be calculated by (Ouchterlony, 2009):

$$b = 0.4\left(\frac{B_{ref}}{B}\right)^{0.25} X_{50}^{0.25} \ln\left(\frac{X_{max}}{X_{50}}\right) \tag{4}$$

where B is the burden, and B_{ref} is the burden reference assumed to be approximately 4 (Segarra Catasús, 2004).

2.1. Mean fragmentation size

2.1.1. Empirical methods

Da Gama (1970) proposed a model for prediction of fragmentation based on the required energy and explosives and rocks characteristics. The main drawback of that model was negligence of spacing effect, bench height, stemming length and lack of uniformity and non-uniformity predictions (Lopez and Lopez, 1995). Due to the impact of several blasting parameters such as specific charge, burden, spacing, nature and rock's discontinuities characteristics, Larson developed another model, which was unable to predict the exact fragmentation as well (Lopez and Lopez, 1995; Hustrulid, 1999). Kuznetsov (1973) presented an empirical model (Eq. (5)) considering the explosives features, nature and variability of rock mass, influence of applied blast energy and evaluation of uniformity and non-uniformity of fragmentation. In this model, the fragmentation is determined in terms of mass percentage, powder factor (applied blast energy per unit volume of rock) and mean fragment size:

$$X_m = Aq^{-0.8}Q_e^{0.167}\left(\frac{115}{E}\right)^{0.633} \quad (5)$$

where X_m is the mean fragment size (cm); A is the rock factor (illustrated in Table 1); Q_e is the mass of explosives used in the hole (kg); E is the ratio of relative weight strength of explosive to ANFO; and q is the powder factor, which can be calculated through the mass of explosives dividing by the volume of rock mass (kg/m^3).

Lilly (1986) presented the blastability index (BI) by considering rock mass fragmentation parameters. Subsequently, Cunningham (1987) revised Kuznetsov model (Eq. (6)) using BI rather than rock factor due to the great influence of rock mass parameters on fragmentation. BI calculated based on Table 2 is written in Eq. (7).

$$X_m = 0.06BI\left(\frac{V_o}{Q_e}\right)^{0.8}Q_e^{0.167}\left(\frac{115}{E}\right)^{0.633} \quad (6)$$

$$BI = 0.5(RMD + JPS + JPA + RDI + HF) \quad (7)$$

where V_o is the rock volume broken per blast hole (m^3).

Kou and Rustan (1993) extended Larson's model named Sve-DeFo and vital parameters including bench height, stemming length, and the discontinuities characteristics and rock's nature were reconsidered. The main disadvantage of their model is assumption of rocks' features in an approximate manner and also the predicted dimensions of fragmented rocks are smaller than the actual value. Morin and Ficarazzo (2006) predicted the size distribution of fragmented rocks using Monte Carlo simulation and Kuz-Ram model based on in situ rock's properties, joint's features, explosives attributes and blasting pattern. A modified Kuz-Ram model was introduced and implemented in Sungun copper mine successfully by Gheibie et al. (2009). Nevertheless, their model was unable to consider the upper limit of particles, which is recognized in the original Kuz-Ram model. Hudaverdi et al. (2012) collected associated information of several mines in Turkey and proposed a statistical model using multi-regression analysis. This model had lower errors compared with the Kuz-Ram model. A model incorporating Rock Engineering Systems (RES) method was proposed by Faramarzi et al. (2013) to predict rock fragmentation in Sungun copper mine in Iran incorporating 16 effective parameters. Their model was compared by regression analysis and Kuz-Ram model. They concluded that the RES approach is more reliable than other two methods. Akbari et al. (2015) predicted rock fragmentation by considering blasting parameters and explosives features. The results of their study demonstrated that various parameters such as joint spacing, discontinuities, uniaxial compressive strength (UCS) of rock and its roughness have a direct relation with the size of fragmented rock.

Table 1
Rock factor values based on rock mass structure (Hustrulid, 1999).

Rock mass condition	Protodyakonov factor	Rock factor, A
Very soft	3–5	3
Soft	5–8	5
Medium soft	8–10	7
Rigid	10–14	10
Rigid and homogenous	12–16	13

Table 2
Rock mass parameters and ratings (Lilly, 1986).

Parameter	Sub-category	Rating
Rock mass description (RMD)	Powdery	10
	Vertically jointed	20
	Massive	50
Joint plane spacing (JPS)	<0.1 m	10
	0.1 m to oversize	20
	Oversize to Pattern size	50
Joint plane angle (JPA)	Horizontal dip	10
	Discontinuity dip out of face	20
	Discontinuity dip perpendicular to face	30
	Discontinuity dip into face	40
Rock density index (RDI)	Density (t/m^3)	25–50
Hardness factor (HF)	If Ym < 50 GPa	UCS/3
	If Ym > 50 GPa	UCS/5

Note: Ym = Young's modulus; UCS = uniaxial compressive strength.

2.1.2. Image analysis

In recent years, image analysis technique has been used for prediction of rock fragmentation by blasting as a high-capability method in mining industry. Al-Thyabat and Miles (2006) predicted particle dimension distribution using watershed algorithm and image analysis technique. Thurley (2011) used three-dimensional (3D) data in order to measure the granular particles of limestone on conveyer belt with the aim of analyzing and evaluating the automatic control of fragmentation process, and their results were improved with respect to the energy efficiency and fragmentation quality. Other researches have been carried out to predict the size distribution and blasting pattern design using GoldSize software (Hosseini and Namvar, 2017), compare fragmentation size distribution through image analysis software and experimental attempts (Sereshki et al., 2016), and develop new fragmentation model using image processing (Elahi and Hosseini, 2017).

2.2. Uniformity index

Uniformity index reflects the uniformity of fragmented rocks' distribution and depends on various geometric and environmental parameters. Cunningham (1983) proposed a new model for prediction of uniformity index value based on Rosin-Rammler model, Kuznetsov model and blasting pattern, in which the value varies between 0.8 and 2.2. This index relies on a number of parameters including hole diameter, burden, spacing in a defined row, drilling accuracy, bench height and charge length, which is written as follows (Cunningham, 1983):

$$n = \left(2.2 - 14\frac{B}{D}\right)\sqrt{\frac{1+\frac{S}{B}}{2}}\left(1-\frac{W}{B}\right)\left(0.1+\frac{|L_b - L_c|}{L}\right)^{0.1}\frac{L}{H}P \quad (8)$$

where D is the hole diameter (mm), L is the length of charging (m), L_b is the downhole charging length (m), L_c is the length of charging in the middle of hole (m), H is the bench height (m), W is the hole's deviation, S is the spacing of holes in a row, and P is the factor of holes' pattern ($P = 1$ for square pattern, and $P = 1.1$ for diamond pattern). In addition, image analysis technique is another approach for prediction of uniformity index which is extensively used for addressing this issue (Hunter et al., 1990).

3. Site description

Jajarm bauxite mine is located in North Khorasan Province, Iran (Fig. 2). The longitudinal extension of this mine from west to east is mostly in the form of layers mainly composed of karstic-dolomites and Elika formations. The physical characteristics of the minerals have a texture consisting of fine pyrolytic and oolitic grains. Generally, the bauxite layer of this mine has four units as follows:

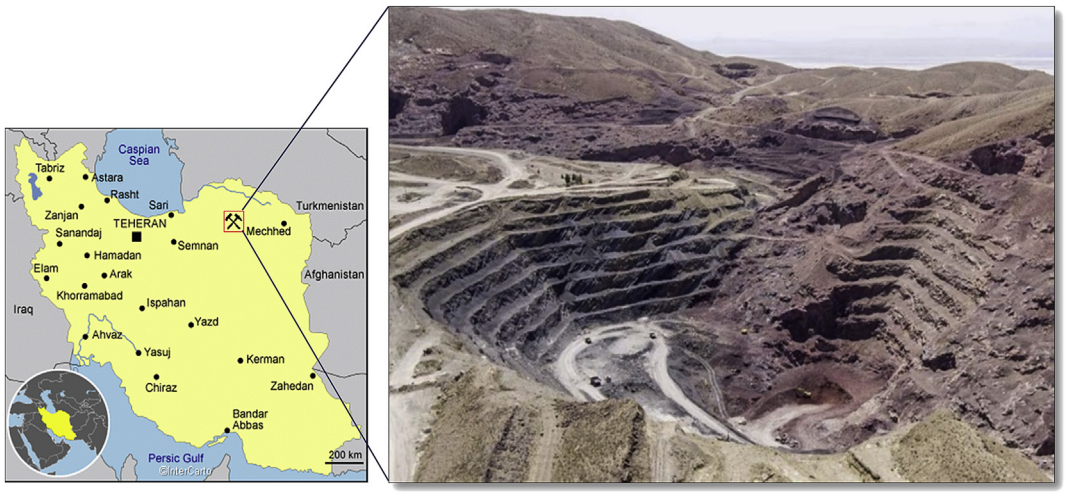

Fig. 2. Jajarm bauxite mine in Iran.

(1) Upper kaolin bauxite (gray to brown in color);
(2) Hard bauxite of brown, light brown, gray, olive green colors;
(3) Soft shale bauxite of reddish brown color; and
(4) Kaolin bauxite of gray to light brown color.

In this study, the data from 24 different blasting operations consisting of burden, hole spacing, powder factor, BI, hole diameter, bench height, hole length, and stemming length were collected (Table 3). In addition, the geomechanical properties of rocks such as UCS, density, and Young's modulus were measured in the laboratory based on the International Society for Rock Mechanics (ISRM) standards (Brown, 1981).

In order to realize the size distribution of blasting operations, the image analysis was carried out by taking several photographs from fragmented muck pile in three steps (after blasting, in the one-third and the two-third of loading by shovel). These photographs were taken randomly in consideration of size variation and two defined scales. In the next step, 15 randomly chosen photographs were selected as the input file for Split-Desktop software, and the outputs including the mean fragmented particles passing from the sieve (X_m), uniformity index (n) and size distribution of fragmented rocks were obtained separately. Fig. 3 shows an example of the main steps adopted in this process. Furthermore, Rosin-Rammler and Swebrec functions were used to predict the size distribution curves as well. Fig. 4 shows one of the randomly chosen photographs attained by these two functions compared with image analysis result.

It can be inferred from Fig. 4 that the range of particle dimensions obtained from the Rosin-Rammler function is closer to that of image analysis than the Swebrec function. Therefore, it is likely that the size distribution of Jajarm bauxite mine follows the Rosin-Rammler function. Therefore, the main purpose of this work is to redefine the variables of the Rosin-Rammler function (i.e. uniformity index and average size) based on the image analysis results.

The statistical description of X_m and n for 24 blasting data are presented in Table 4. It can be seen that there is a meaningful difference between the values obtained by image analysis and Rosin-Rammler function. In other words, the size distribution measured by this function is greater than other values and vice versa.

4. Methodology

There is a significant difference between the results obtained from empirical methods and image analysis due to the fact that empirical models are considered as a site-dependent technique. Thus, the existing prediction model was modified in this study, and a new one was proposed for Jajarm bauxite mine using regression and DEMATEL approaches. Since blasting operations in open pit mines are site-dependent, the comparison of these two approaches, in which the first one is based on the actual data obtained from blasting sites and the second one relies on experts' knowledge and experience, can be useful for determination of the best results.

4.1. Statistical approach

Regression analysis is a set of statistical processing methods for determination of relationship among various variables. The relationship between variables may be either linear or nonlinear. Generally, regression processing is divided into four main steps including variable selection, data collection, identification and model fitting, and validation (Ghiasi et al., 2016).

Table 3
Statistical parameters of collected data.

Statistical parameter	Burden, B (m)	Hole spacing, S (m)	Hole diameter, D (mm)	Hole length, L (m)	Bench height, H (m)	Blastability index, BI	Powder factor, Pf (kg/m^3)	Stemming length, T (m)
Minimum	1.8	2	63	2.8	6	71.3	0.226	0.1
Maximum	3	3.5	76	4.74	7	81.3	0.62	1.25
Mean	2.31	2.62	71.71	3.98	6.71	77.456	0.401	0.66
Standard deviation	0.51	0.56	5.13	0.65	0.45	3.23	0.142	0.33

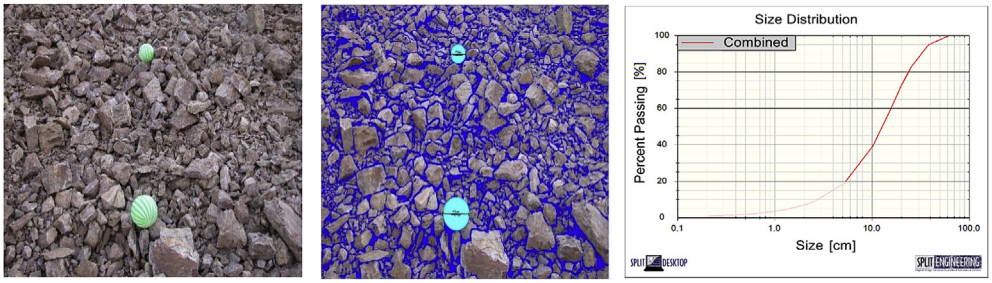

Fig. 3. Image analysis process: (a) A randomly chosen photograph; (b) Fragmentation analysis in Split-Desktop software; and (c) Obtained curve for size distribution.

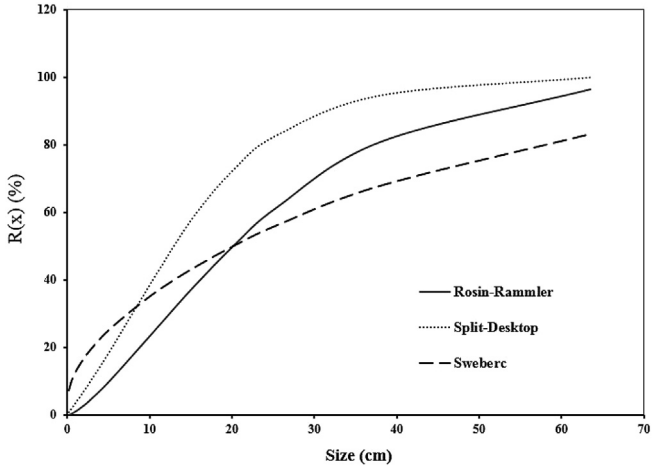

Fig. 4. Comparison of size distributions curves.

Table 4
Comparison of n and X_m values obtained from Rosin-Rammler function and image analysis.

Statistical parameter	n		X_m (cm)	
	Image analysis	Rosin-Rammler	Image analysis	Rosin-Rammler
Minimum	0.62	0.82	7.18	11.74
Maximum	1.43	1.37	22.4	29.15
Mean	1.048	1.07	14.24	21.41
Standard deviation	0.26	0.163	4.83	5.93

4.1.1. Linear regression model

Linear multiple variable model is a kind of linear regression model, which can be described by Eq. (9). This equation is fitted to dependent variables using the least squares approach (Weisberg, 2005).

$$Y = \beta_0 + \beta_1 X_1 + \beta_2 X_2 + \cdots + \beta_n X_n + \varepsilon \tag{9}$$

where Y is the independent variable; X_1, X_2, …, X_n are the dependent variables; β_1, β_2, …, β_n are the coefficients for dependent variables; β_0 is the constant value; and ε is the sum of random errors. Due to the complexity of calculations, SPSS software was used to facilitate the statistical processing.

4.1.2. Nonlinear regression model

The basic of nonlinear regression relies on linear regression. In other words, it is a form of regression processing which can be obtained by a nonlinear function combination set of dependent and independent variables without consideration of linear constraints. This kind of regression has several models that can be categorized into exponential, quadratic, power and other types. In general, nonlinear regression model can be defined as (Tiryaki, 2008):

$$Y = aX_1^{b_1} X_2^{b_2} X_3^{b_3} \cdots X_n^{b_n} \tag{10}$$

where a is the intercept; and b_1, b_2, …, b_n are the regression coefficients. This equation can be rewritten to a linear logarithmic function (Eq. (11)) by transformation of both sides to logarithmic scale and a linear regression function (Eq. (12)) (Tiryaki, 2008):

$$\log_{10} Y = \log_{10} a + b_1 \log_{10} X_1 + \cdots + b_n \log_{10} X_n \tag{11}$$

$$Y' = a' + b_1' X_1 + b_2' X_2 + \cdots + b_n' X_n \tag{12}$$

4.2. DEMATEL technique

DEMATEL is a graph theory based technique. It is practical and useful method for visualizing the structure of complicated causal relations with matrices or directed graphs (Fontela and Gabus, 1972, 1976). It can model the interdependence relations within a set of criteria under consideration. This method can provide a visual structural model by altering the relationships between cause and effect of the evaluation criteria.

In order to use DEMATEL, the following main steps should be done (Si et al., 2018).

(1) Step 1: generate the average matrix

Experts indicate the direct influence that each factor exerts on the others according to an integer scale range: 0 (no influence), 1 (very low influence), 2 (low influence), 3 (high influence), and 4 (very high influence). If there are h experts and n factors, each expert makes the $n \times n$ non-negative matrix $\boldsymbol{X}_k$ ($1 \le k \le h$). Hence, $\boldsymbol{X}_1, \boldsymbol{X}_2, \ldots, \boldsymbol{X}_h$ are the resulting matrices for each of the h experts, and each element of $\boldsymbol{X}_k$ is an integer, denoted as x_{ij}^k that shows the direct influence of factor i on factor j based on the opinion of the kth expert. Obviously, diagonal elements that show the influence of each parameter on itself are equal to zero. The average matrix $\boldsymbol{A}$ of direct influence can be calculated by averaging the h expert's value matrices. The (i, j) element of the matrix $\boldsymbol{A}$ is a_{ij} and calculated as follows:

$$a_{ij} = \frac{1}{h} \sum_{k=1}^{h} x_{ij}^k \tag{13}$$

(2) Step 2: calculate the normalized direct influence matrix

The normalized direct influence matrix $\boldsymbol{D}$ is obtained through normalizing the matrix $\boldsymbol{A}$ as follows:

$$\boldsymbol{D} = s\boldsymbol{A} \tag{14}$$

where s is a constant and can be written as follows:

$$s = \min\left(\frac{1}{\max_{1\le i\le n}\sum_{j=1}^{n} a_{ij}}, \frac{1}{\max_{1\le j\le n}\sum_{i=1}^{n} a_{ij}}\right) \ (i,j = 1,2,\cdots,n) \tag{15}$$

(3) Step 3: derive the total relation matrix

A continuous decrease of the indirect effects of problems along the powers of matrix $\boldsymbol{D}$ (e.g. $\boldsymbol{D}^2$, $\boldsymbol{D}^3$, …, $\boldsymbol{D}^{+\infty}$) guarantees convergent solutions to the matrix inversion, similar to an absorbing Markov chain matrix. Therefore, the total relation matrix $\boldsymbol{T}$ is an $n \times n$ matrix and derived as follows:

$$\begin{aligned}\boldsymbol{T} &= \sum_{m=1}^{+\infty} \boldsymbol{D}^i = \boldsymbol{D} + \boldsymbol{D}^2 + \boldsymbol{D}^3 + \cdots + \boldsymbol{D}^{+\infty} = \boldsymbol{D}(\boldsymbol{I} - \boldsymbol{D})^{-1}(\boldsymbol{I} - \boldsymbol{D}^m) \\ &= \boldsymbol{D}(\boldsymbol{I} - \boldsymbol{D})^{-1}\end{aligned} \tag{16}$$

where $\boldsymbol{I}$ is the identity matrix. The (i, j) element of the matrix $\boldsymbol{T}$, t_{ij}, denotes the full direct/indirect influence exerted from factor x_i to factor x_j. The vectors $\boldsymbol{r}$ and $\boldsymbol{c}$, representing the sum of the rows and the sum of the columns from the total-influence matrix $\boldsymbol{T}$, respectively, obtained as

$$\boldsymbol{r} = [r_i]_{1\times n} = \left(\sum_{j=1}^{n} t_{ij}\right)_{n\times 1} \tag{17}$$

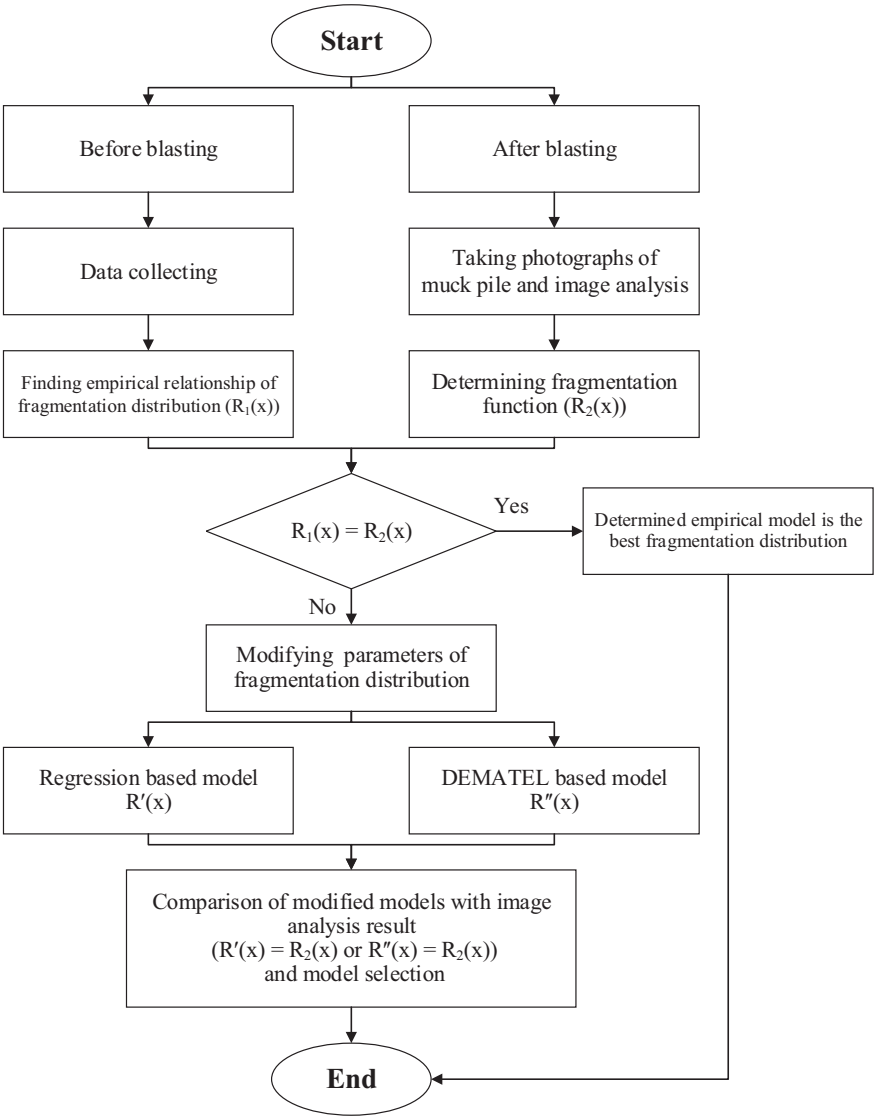

Fig. 5. Flowchart of proposed framework.

Table 5
Developed regression models.

n'			X'_m(cm)		
RMSE	R^2	Model	RMSE (cm)	R^2	Model
0.072	0.935	$n' = 3.861 + 1.9Pf - 0.011BI - 2.247\frac{S}{B} + 12.54\frac{B}{D} + 0.32\frac{L}{H}$	3.488	0.99	$X'_m = 10^{-2.342}\left(\frac{S}{B}\right)^{2.442} T^{-0.067} Dr^{3.083}\left(\frac{RQD}{J_n}\right)^{0.285} X_m^{0.845}\left(\frac{H}{B}\right)^{1.021}$
0.08	0.925	$n' = 3.538 + 1.507Pf - 0.01BI - 1.416\frac{S}{B} + 0.012\frac{H}{B}$	1.781	0.929	$X'_m = 10^{-1.021}\left(\frac{H}{B}\right)^{1.131}\left(\frac{T}{B}\right)^{0.065} Dr^{2.371}\left(\frac{RQD}{J_n}\right)^{0.113} X_m^{0.77}\left(\frac{B}{D}\right)^{0.451}$
0.086	0.929	$n' = 3.821 + 1.86Pf - 0.01BI - 2.037\frac{S}{B} + 9.756\frac{B}{D}$	0.909	0.91	$X'_m = 10^{-0.965}\left(\frac{H}{B}\right)^{1.061} Dr^{2.372}\left(\frac{RQD}{J_n}\right)^{0.11} X_m^{0.758} T^{-0.055}\left(\frac{B}{D}\right)^{0.437}$
0.086	0.912	$n' = 2.521 - 0.227\frac{S}{B} + 0.508\frac{H}{B} + 11.371\frac{B}{D} - 0.004BI - 0.372H$	3.276	0.887	$X'_m = -42.609 + 4.805\frac{H}{B} - 5.730\frac{T}{B} + 8.09Dr + 0.108\frac{RQD}{J_n} 0.659X_m + 145.916\frac{B}{D}$
0.086	0.904	$n' = 1.138 + 0.563Pf + 0.265\frac{H}{B} + 0.001\frac{S}{B} - 0.163H$	4.047	0.971	$X'_m = -73.23 + 25.235\frac{S}{B} + 4.077\frac{H}{B} - 2.517T + 10.568Dr + 0.247\frac{RQD}{J_n} + 0.659X_m$
			3.123	0.901	$X'_m = -40.493 + 4.277\frac{H}{B} - 2.386T + 7.994Dr + 0.115\frac{RQD}{J_n} + 0.630X_m + 145.916\frac{B}{D}$

Note: RQD = rock quality designation; J_n = joint set number; Dr = density of rock.

Table 6
Matrix ***A*** for uniformity index.

Element	S/B	H/B	B/D	RQD/J_n	BI
S/B	0	1.25	2	0.25	0.75
H/B	1.5	0	2.25	0.5	1.75
B/D	2.25	1.75	0	0.75	2.25
RQD/J_n	1.75	1.5	1.75	0	2
BI	1.75	2.25	2	0.5	0

Table 7
Matrix ***A*** for mean fragment size.

Element	S/B	H/B	B/D	T/B	TD	BHP	NR	RQD/J_n	BI	L/H
S/B	0	1.25	2	1	3.25	3	3.25	0.25	0.75	1.75
H/B	1.5	0	2.25	2	2.5	2.75	2.5	0.5	1.75	2
B/D	2.25	1.75	0	1.75	2.5	2.75	1.5	0.75	2.25	1.5
T/B	0.5	1.25	1	0	1	2	0.75	0.75	1.5	1.25
TD	1.75	1.5	1.75	1.25	0	0.75	1.25	1.5	2	1.25
BHP	1.75	1.25	2.5	2	3	0	2.25	1	2	1.75
NR	1.25	1.75	1.75	2	2.5	2.75	0	0.5	1	1.25
RQD/J_n	2.5	2.25	2.5	2.25	1.5	3.5	1.5	0	3	1.5
BI	1.75	2.25	2	1.75	1.75	2.75	1.25	0.5	0	3
L/H	0.75	1	1.25	2.25	1.75	1.75	1	1.5	0.75	0

Note: TD = time delay; BHP = blast hole pattern; NR = number of rows.

Table 8
Matrix ***D*** for uniformity index.

Element	S/B	H/B	B/D	RQD/J_n	BI
S/B	0	0.15625	0.25	0.03125	0.09375
H/B	0.1875	0	0.28125	0.0625	0.21875
B/D	0.28125	0.21875	0	0.09375	0.28125
RQD/J_n	0.21875	0.1875	0.21875	0	0.25
BI	0.21875	0.28125	0.25	0.0625	0

$$\boldsymbol{c} = [c_j]_{1\times n} = \left(\sum_{i=1}^{n} t_{ij}\right)_{1\times n} \tag{18}$$

where r_i is the ith row sum in the matrix ***T*** and displays the sum of the direct and indirect effects dispatching from factor i to the other factors. Similarly, c_j is the jth column sum in the matrix ***T*** and depicts the sum of direct and indirect effects that factor j is receiving from the other factors.

5. Proposed framework

As described before, Rosin-Rammler function is based on geomechanical and geometric parameters. Geomechanical parameters rely on environmental features and geometric parameters depend on physical conditions and behaviors. For this reason, most of the tectonic parameters (e.g. discontinuities spacing, orientations and dip) do not hold in this relationship and as a result, the Rosin-Rammler function does not guarantee size distribution precisely (Bhandari, 1997; Gheibie et al., 2009). Also, in uniformity index (Eq. (8), none of the environmental parameters are present. Meanwhile, the uniformity index depends on environmental characteristics. Thus, the proposed models for uniformity index such as Lilly (1986) are based on geometric parameters.

According to the collected blasting data, 20 blasting data were selected as training datasets and 4 blasting data for validation purposes. Fig. 5 shows the flowchart of proposed framework.

5.1. Regression model

In order to evaluate the size distribution of blasting in this mine, the input parameters of Rosin-Rammler function were utilized with linear and nonlinear multiple variable regressions.

Table 9
Matrix ***D*** for mean fragment size.

Element	S/B	H/B	B/D	T/B	TD	BHP	NR	RQD/J_n	BI	L/H
S/B	0	0.056	0.09	0.045	0.147	0.136	0.147	0.011	0.034	0.079
H/B	0.068	0	0.102	0.09	0.113	0.125	0.113	0.022	0.079	0.09
B/D	0.102	0.079	0	0.079	0.113	0.125	0.068	0.034	0.102	0.068
T/B	0.022	0.056	0.045	0	0.045	0.09	0.034	0.034	0.068	0.056
TD	0.079	0.068	0.079	0.056	0	0.034	0.056	0.068	0.09	0.056
BHP	0.079	0.056	0.113	0.09	0.136	0	0.102	0.045	0.09	0.079
NR	0.056	0.079	0.079	0.09	0.113	0.125	0	0.022	0.045	0.056
RQD/J_n	0.113	0.102	0.113	0.102	0.068	0.159	0.068	0	0.136	0.068
BI	0.079	0.102	0.09	0.079	0.079	0.125	0.056	0.022	0	0.136
L/H	0.034	0.045	0.056	0.102	0.079	0.079	0.045	0.068	0.034	0

Table 10
Matrix ***T*** for uniformity index.

Element	*S/B*	*H/B*	*B/D*	RQD/J_n	BI
S/B	0.43	0.536	0.666	0.17	0.481
H/B	0.735	0.544	0.848	0.243	0.706
B/D	0.863	0.786	0.7	0.285	0.802
RQD/J_n	0.836	0.778	0.893	0.208	0.802
BI	0.788	0.797	0.865	0.252	0.554

Table 11
Matrix ***T*** for mean fragment size.

Element	*S/B*	*H/B*	*B/D*	*T/B*	TD	BHP	NR	RQD/J_n	BI	*L/H*
S/B	0.157	0.211	0.274	0.225	0.361	0.350	0.307	0.103	0.2	0.243
H/B	0.231	0.169	0.296	0.278	0.344	0.359757	0.287	0.119	0.252	0.267
B/D	0.258	0.239	0.199	0.262	0.339	0.354	0.246	0.125	0.268	0.245
T/B	0.124	0.155	0.165	0.117	0.186	0.232	0.143	0.090439	0.172	0.165
TD	0.205	0.196	0.231	0.203	0.184	0.23	0.197	0.135	0.223	0.198
BHP	0.24	0.223	0.303	0.275	0.359	0.245	0.274	0.138	0.261	0.255
NR	0.19	0.216	0.245	0.247	0.306	0.319	0.156	0.104	0.196	0.208
RQD/J_n	0.305	0.296	0.346	0.324	0.35	0.440	0.286	0.110	0.337	0.286
BI	0.234	0.255	0.279	0.262	0.306	0.351	0.233	0.116	0.171	0.302
L/H	0.150	0.162	0.194	0.229	0.23	0.246	0.169	0.131	0.161	0.126

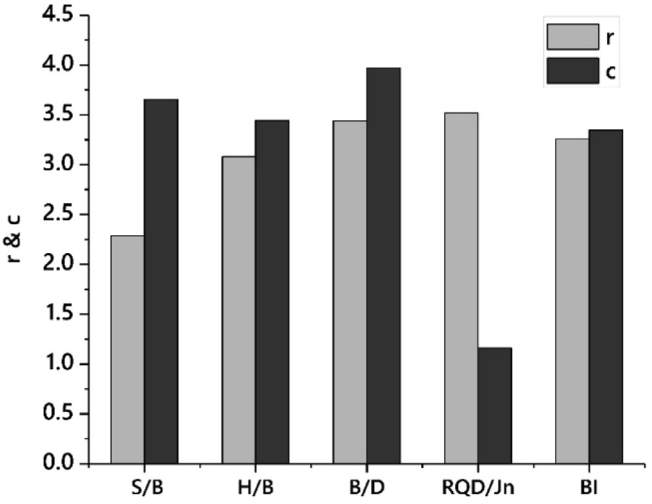

Fig. 6. The ***r*** and ***c*** vectors for uniformity index.

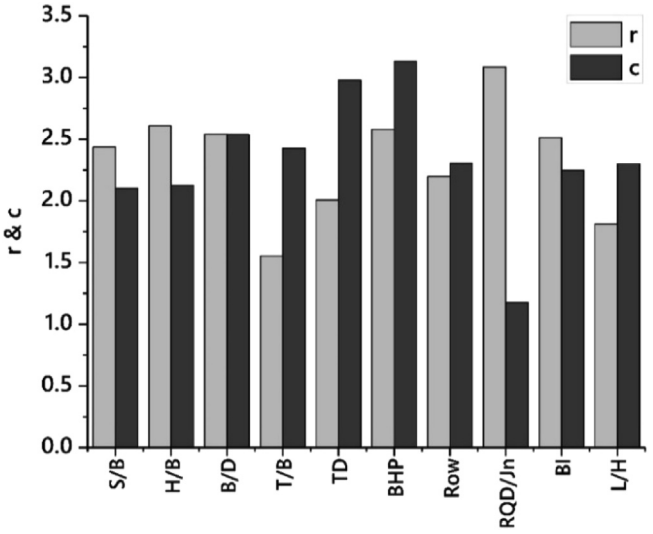

Fig. 7. The ***r*** and ***c*** vectors for mean fragment size.

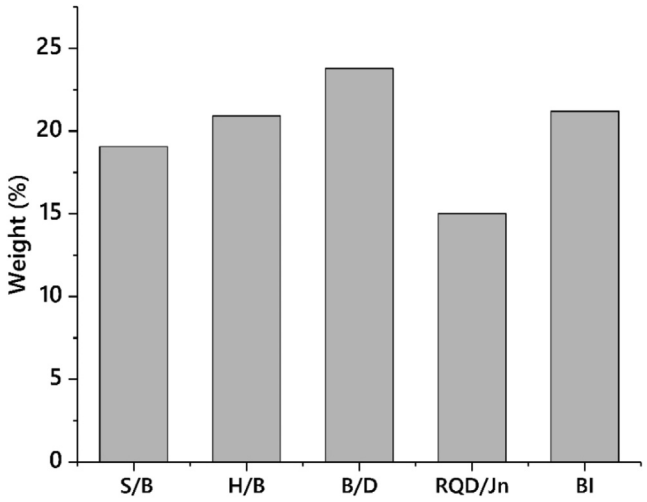

Fig. 8. Parameter weights of uniformity index.

At the first step, all effective parameters in the Jajarm bauxite mine were considered carefully. After that, using SPSS software, a variety of available scenarios based on input data were determined using their correlation and normalization. Consequently, 116 and 84 possible equations were generated for uniformity index (n') and mean fragment size (X'_m), respectively. At the final step, based on a predefined procedure, 5 models for the uniformity index as well as 6 models for the mean fragment size were proposed based on the performance criteria (i.e. coefficient of determination (R^2) and the root mean square error (RMSE)) to improve the size distribution of fragmented rocks obtained by Rosin-Rammler function (Table 5).

5.2. DEMATEL based model

In order to incorporate the DEMATEL method for evaluation and prediction of rock fragmentation, 13 questionnaires were distributed among mine experts. These questionnaires contain two main matrixes: one for measuring small dimensions and the other for uniformity index.

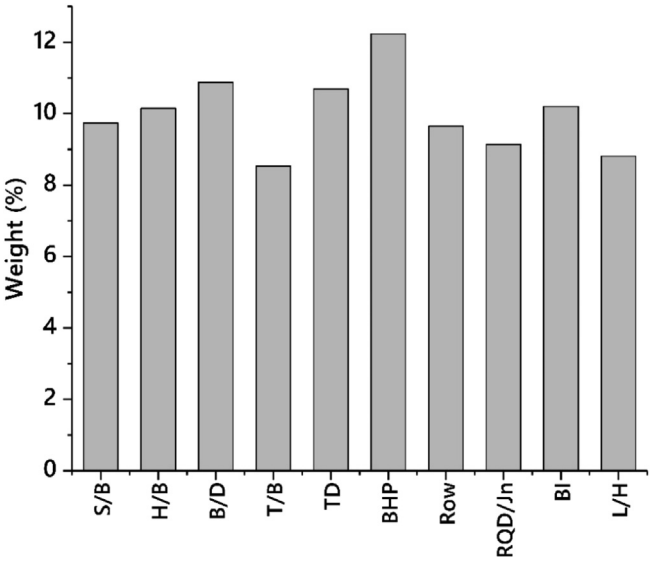

Fig. 9. Parameter weights of mean fragment size.

Table 12
Rating table of effective parameters in blasting operation.

BI		S/B		B/D		L/H		H/B		T/B		RQD/J_n		NR		TD (ms)		BHP	
Value	Rating	Value	Rating	Value	Rating	Value	Rating	Value	Rating	Value	Rating	Value	Rating	Value	Rating	Value	Rating	Description	Rating
0–20	4	<1.056	0	<30.84	3	<0.491	3	<2.64	0	<0.165	0	<10.083	1	<6	4	<2	0	Staggered	3
21–40	3	[1.056, 1.12)	3	[30.84, 35.38)	2	[0.491, 0.5833)	2	[2.64, 2.96)	1	[0.165, 0.28)	2	[10.083, 13.5)	3	[6, 9)	3	[2, 4)	1	Square	2
41–60	2	[1.12, 1.16)	2	[35.38, 39.91)	1	[0.5833, 0.675)	1	[2.96, 3.27)	2	[0.28, 0.39)	4	[13.5, 16.91)	4	[9, 11)	2	[4, 6)	3	Rectangular	1
61–80	1	[1.16, 1.22)	1	≥39.91	0	≥0.675	0	[3.27, 3.58)	3	[0.39, 0.51)	3	[16.91, 20.34)	2	[11, 14)	1	[6, 7)	4	Single row	0
81–100	0	≥1.22	0					≥3.58	4	≥0.51	1	≥20.34	0	≥14	0	[7, 9)	2		

Table 13
Developed DEMATEL-based models.

n'''				X'''_m(cm)			
Type	RMSE (cm)	R^2	Model	Type	RMSE (cm)	R^2	Model
Exponential	0.16	0.737	$n''' = 0.5855\exp(0.01161n_i)$	Exponential	2.058	0.737	$X'''_m = 3.176\exp(0.0225X_{mi})$
Exponential	0.178	0.754	$n''' = -3.315\times10^{13}\exp(-1.838n_i)+0.6274\exp(0.0105n_i)$	Exponential	2.015	0.811	$X'''_m = 4.559\exp(0.0178X_{mi})-4.184\times10^{9}\exp(-0.4181X_{mi})$
Fourier	0.184	0.737	$n''' = 1.176-0.4764\cos(0.02853n_i)-0.057\sin(0.02853n_i)$	Fourier	2.171	0.781	$X'''_m = -2.694\times10^{7}+2.694\times10^{7}\cos(-1.832\times10^{-5}X_{mi})-5.078\times10^{4}\sin(-1.832\times10^{-5}X_{mi})$
Gaussian	0.171	0.736	$n''' = 1.641\times10^{4}\exp\{-[(n_i-1716)/536.2]^2\}$	Gaussian	2.055	0.771	$X'''_m = 20.11\exp\{-[(X_{mi}-89.28)/44.07]^2\}$
Polynomial	0.161	0.732	$n''' = 0.01182n_i+0.4828$	Polynomial	1.937	0.767	$X'''_m = 0.337X_{mi}-7.559$
Polynomial	0.171	0.737	$n''' = 7.145\times10^{-5}n_i^2+0.0051n_i+0.6085$	Polynomial	2.01	0.781	$X'''_m = -0.0045X_{mi}^2+0.9301X_{mi}-26.41$
Polynomial	0.184	0.737	$n''' = -1.382\times10^{-6}n_i^3+0.0002n_i^2-0.002n_i+0.7003$	Power	1.976	0.758	$X'''_m = 0.02606X_{mi}^{1.508}$
Power	0.165	0.717	$n''' = 0.1555n_i^{0.4998}$	Power	1.988	0.786	$X'''_m = -2974X_{mi}^{-1.239}+31.95$
Power	0.171	0.737	$n''' = 0.0009n_i^{1.537}+0.6419$				

By undertaking step 1 in the DEMATEL method, the average matrices of uniformity index and mean fragment size were generated as shown in Tables 6 and 7, respectively.

The maximum sums of the rows and columns in Tables 6 and 7 are equal to 8 and 22.5, respectively. Accordingly, constant values of s are 1/8 and 1/22.5 and thus the normalized direct influence matrices were calculated in Tables 8 and 9 for uniformity index and mean fragment size, respectively. The total relation matrix using Eq. (16) was calculated and the results are listed in Tables 10 and 11.

Based on the elements of matrices $\boldsymbol{T}$, the $\boldsymbol{r}$ and $\boldsymbol{c}$ vectors are calculated and demonstrated in Figs. 6 and 7 for uniformity index and mean fragment size, respectively.

Ultimately, the weights of all parameters are computed using Eq. (19) and are illustrated in Figs. 8 and 9.

$$w_i = \frac{r_i + c_i}{\sum_{i=1}^{n} r_i + \sum_{i=1}^{n} c_i} \tag{19}$$

In order to define DEMATEL-based n and X_m, all the parameters involved were classified into some classes in accordance with their role in the blasting on the basis of the literature and analytical studies. A corresponding rating from 0 to 4 was assigned to each class. Table 12 shows the proposed ratings of the effective parameters in blasting operation.

The DEMATEL-based n and X_m, called uniformity index (n_i) and mean fragment size index (X_{mi}), respectively, are defined as

$$n_i = \sum_{i=1}^{7} w_i \frac{P_i}{P_{max}} \tag{20}$$

$$X_{mi} = \sum_{i=1}^{7} w_i \frac{P_i}{P_{max}} \tag{21}$$

where w_i is the weight of the ith parameter, P_i is the rate of the ith parameter (0–4), and P_{max} is the maximum rate of the ith parameter.

In order to investigate the relationship between uniformity and mean fragment size (i.e. n''' and X'''_m, respectively) obtained from the image analysis and the DEMATEL-based indices (i.e. Eqs. (20) and (21)), the curve fitting approach was applied. For this purpose, several curves were fitted by the data, and their RMSE and R^2 values were calculated and listed in Table 13.

It can be inferred from Table 13 that exponential model for uniformity index and polynomial model for mean fragment size have the lowest RMSE and highest R^2, respectively. Thus, these two proposed equations were selected as the DEMATEL-based models of n and X_m.

6. Evaluation of proposed models

Capabilities of the proposed models were evaluated on four blasting cases. Table 14 and Fig. 10 illustrate the prediction of uniformity index and mean fragment size using proposed models. In addition, the fragmentation distributions resulting from image analysis, conventional Rosin-Rammler function and modified Rosin-Rammler function via regression model and DEMATEL based model are plotted in Fig. 11.

It can be seen from Table 14 and Fig. 10 that regression model has closer results to the image analysis for the uniformity index and the mean fragment size in comparison with other models. Subsequently, the fragmentation distribution obtained via regression is more consistent with image analysis results, as depicted in Fig. 11.

Four criteria (R^2, RMSE, VAF (value account for) and MAPE (mean absolute percentage error)) were used for the sake of quantitative comparison. Smaller RMSE values produce higher coefficients of determination, leading to more accurate fitted curves. In the same direction, higher VAF values and smaller MAPE values are desired for fitted relationships. The calculated values of these indices for the proposed models are given in Table 15.

Table 14
Prediction results of uniformity index and mean fragment size.

Blast No.	n				X_m (cm)			
	Image analysis	Rosin-Rammler	DEMATEL model	Regression model	Image analysis	Rosin-Rammler	DEMATEL model	Regression model
B21	1.24	0.9569	1.041	1.1942	19.1	29.15	11.054	20.02
B22	0.86	1.005	1.052	0.911	13.14	28.49	10.47	15.7081
B23	0.75	0.8221	1.148	0.7807	22.4	28.68	11.089	20.39121
B24	1.24	1.094	0.942	1.215	22.39	25.3	13.903	23.6336

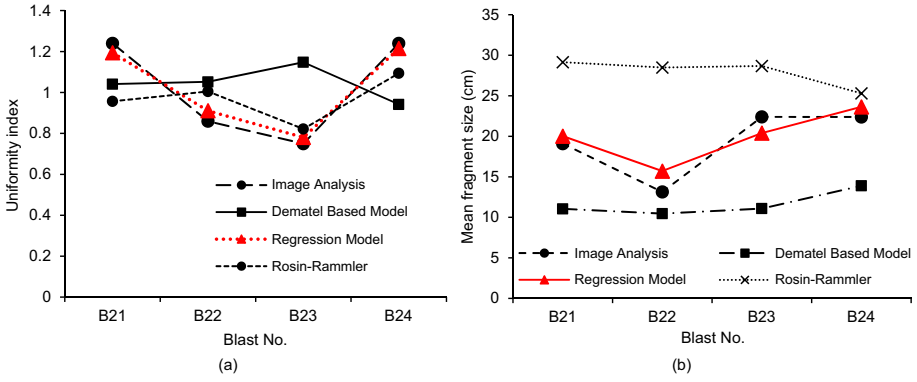

Fig. 10. Comparisons between measured and predicted values: (a) Uniformity index, and (b) mean fragment size.

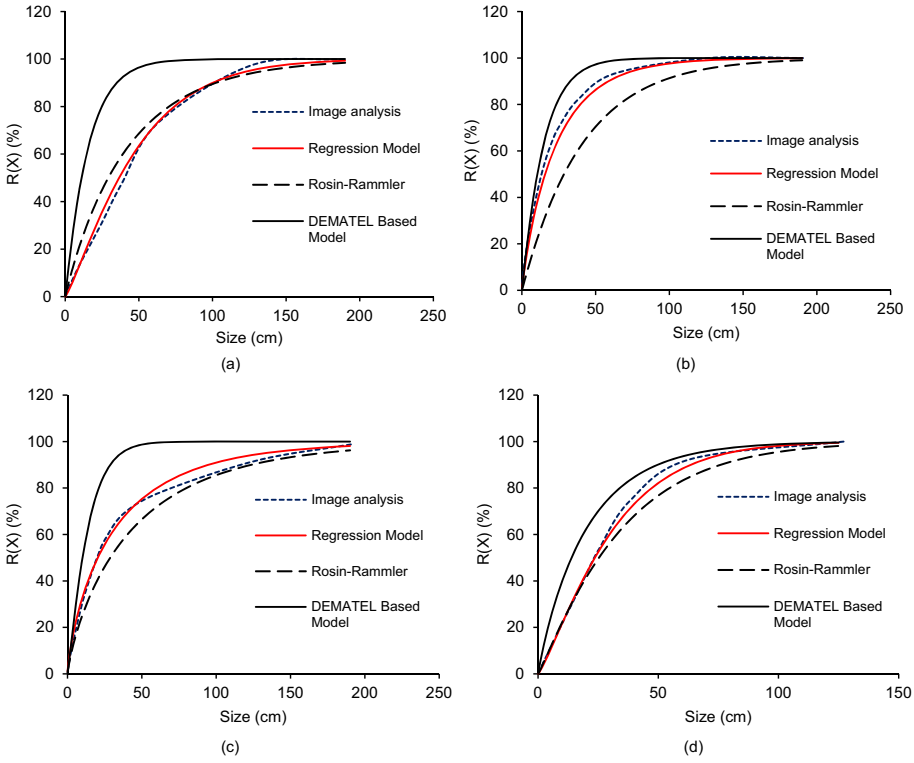

Fig. 11. Comparisons between measured and predicted fragmentation distributions: (a) B21, (b) B22, (c) B23, and (d) B24.

Table 15
Calculated performance criteria for proposed models.

Model	n				X_m (cm)			
	RMSE	R^2	VAF (%)	MAPE (%)	RMSE (cm)	R^2	VAF (%)	MAPE (%)
DEMATEL	0.284	0.6625	64.66	8.87	8.24	0.897	31.63	37.71
Regression	0.04744	0.9936	96.455	5.693	1.771	0.9343	91.71	16.57

According to the visual comparison (Figs. 10 and 11) and performance criteria, it could be deduced that the Rosin-Rammler based on the regression models was capable of predicting fragmentation distribution with a reasonable accuracy.

7. Conclusions

In this paper, a new framework was proposed to predict fragmentation size distribution caused by blasting operation in open pit mining. The proposed framework was developed on the basis of image analysis and incorporating regression and DEMATEL methods in a case study. The main conclusions were drawn from this study as follows:

(1) The analysis based on the DEMATEL method shows that B/D and BHP are the most effective parameters on the uniformity index and mean fragmentation size, respectively.
(2) The Rosin-Rammler function was more in line with image analysis results compared to other empirical models.
(3) The regression model was found to be superior in comparison with the DEMATEL based model to predict the uniformity index with R^2 and RMSE values of 0.9936 and 0.0474, respectively.
(4) The regression model possessed a higher performance in prediction of the mean fragmentation size when compared to the DEMATEL based model with R^2 and RMSE values of 0.9343 and 1.771, respectively.
(5) Modification of the Rosin-Rammler function incorporating regression model which was developed on the basis of field data calculated accurately the fragmentation size distribution in accordance with image analysis method.

Conflicts of interest

We wish to confirm that there are no known conflicts of interest associated with this publication and there has been no significant financial support for this work that could have influenced its outcome.

References

Akbari M, Lashkaripour G, Bafghi AY, Ghafoori M. Blastability evaluation for rock mass fragmentation in Iran central iron ore mines. International Journal of Mining Science and Technology 2015;25(1):59–66.
Al-Thyabat S, Miles NJ. An improved estimation of size distribution from particle profile measurements. Powder Technology 2006;166(3):152–60.
Bhandari S. Engineering rock blasting operations. A.A. Balkema; 1997.
Brown ET. Rock characterization, testing & monitoring: ISRM suggested methods. International Society for Rock Mechanics (ISRM); 1981.
Chakraborty AK, Raina AK, Ramulu M, Choudhury PB, Haldar A, Sahu P, Bandopadhyay C. Parametric study to develop guidelines for blast fragmentation improvement in jointed and massive formations. Engineering Geology 2004;73(1–2):105–16.
Cunningham C. The Kuz-Ram model for production of fragmentation from blasting. In: Proceedings of the 1st Symposium on Rock Fragmentation by Blasting; 1983. p. 439–53.
Cunningham CVB. Fragmentation estimations and the Kuz-Ram model-Four years on. In: Proceedings of the 2nd International Symposium on Rock Fragmentation by Blasting; 1987. p. 475–87.

Da Gama CD. Laboratory studies of comminution in rock blasting. PhD Thesis. University of Minnesota; 1970.
Djordjevic N. Optimal blast fragmentation. Mining Magazine 1998;178(2):121–5.
Elahi AT, Hosseini M. Analysis of blasted rocks fragmentation using digital image processing (case study: limestone quarry of Abyek Cement Company). International Journal of Geo-Engineering 2017;8(1):16. https://doi.org/10.1186/s40703-017-0053-z.
Faramarzi F, Mansouri H, Farsangi ME. A rock engineering systems based model to predict rock fragmentation by blasting. International Journal of Rock Mechanics and Mining Sciences 2013;60:82–94.
Fontela E, Gabus A. The DEMATEL observer. Geneva, Switzerland: Battelle Institute, Geneva Research Center; 1976.
Fontela E, Gabus A. World problems: An invitation to further thought within the framework of DEMATEL. Technical report. Geneva, Switzerland: Battelle Institute, Geneva Research Centre; 1972.
Gheibie S, Aghababaei H, Hoseinie SH, Pourrahimian Y. Modified kuz-ram fragmentation model and its use at the Sungun copper mine. International Journal of Rock Mechanics and Mining Sciences 2009;46(6):967–73.
Ghiasi M, Askarnejad N, Dindarloo SR, Shamsoddini H. Prediction of blast boulders in open pit mines via multiple regression and artificial neural networks. International Journal of Mining Science and Technology 2016;26(2):183–6.
Hosseini M, Namvar ZN. The design of the large blastholes pattern by analyzing of fragmentation of blasted rocks in Sarcheshmeh Copper Mine. Geotechnical and Geological Engineering 2017;35(1):395–402.
Hudaverdi T, Kuzu C, Fisne A. Investigation of the blast fragmentation using the mean fragment size and fragmentation index. International Journal of Rock Mechanics and Mining Sciences 2012;56:136–45.
Hunter GC, McDermott C, Miles NJ, Singh A, Scoble MJ. A review of image analysis techniques for measuring blast fragmentation. Mining Science and Technology 1990;11(1):19–36.
Hustrulid W. Blasting principles for open-pit blasting: Theoretical foundations. Rotterdam: A.A. Balkema; 1999.
Kanchibotla SS, Morrell S, Valery W, O'Loughlin P. Exploring the effect of blast design on SAG mill throughput at KCGM. In: Proceedings of the Mine to Mill Conference; 1998. p. 153–8.
Kojovic T, Michaux S, McKenzie C. Impact of blast fragmentation on crushing and screening operations in quarrying. In: Proceedings of the EXPLO 1995 Conference. Brisbane; 1995. p. 427–35.
Kou S, Rustan A. Computerized design and result prediction of bench blasting. In: Proceedings of the International Symposium on Rock Fragmentation by Blasting; 1993. p. 263–71.
Kuznetsov VM. The mean diameter of the fragments formed by blasting rock. Soviet Mining 1973;9(2):144–8.
Lilly PA. An empirical method of assessing rock mass blastability. Australasian Institute of Mining and Metallurgy; 1986.
Lopez JC, Lopez JE. Drilling and blasting of rocks. Rotterdam: A.A. Balkema; 1995.
Michaux S, Djordjevic N. Influence of explosive energy on the strength of the rock fragments and SAG mill throughput. Minerals Engineering 2005;18(4):439–48.
Monjezi M, Dehghani M, Dehghani H. Optimization of blast pattern using neural networks in Chandermoul iron ore mine. In: Proceedings of the 26th International Geosciences Congress; 2008 [in Persian].
Monjezi M, Rezaei M, Varjani AY. Prediction of rock fragmentation due to blasting in Gol-E-Gohar iron mine using fuzzy logic. International Journal of Rock Mechanics and Mining Sciences 2009;46(8):1273–80.
Morin MA, Ficarazzo F. Monte Carlo simulation as a tool to predict blasting fragmentation based on the Kuz-Ram model. Computers and Geosciences 2006;32(3):352–9.
Nielsen K, Kristiansen J. Blasting and grinding-An integrated comminution system. In: Proceedings of EXPLO 1995 Conference. Brisbane; 1995. p. 113–7.
Ouchterlony F. Fragmentation characterization: the Swebrec function and its use in blast engineering. In: Proceedings of the International Symposium on Rock Fragmentation by Blasting. CRC Press; 2009. p. 3–22.
Ouchterlony F. The Swebrec function: linking fragmentation by blasting and crushing. Mining Technology 2005a;114(1):29–44.
Ouchterlony F. What does the fragment size distribution of blasted rock look like? In: Proceedings of the EFEE World Conference on Explosives and Blasting. European Federation of Explosives Engineers; 2005b. p. 189–99.
Rosin R, Rammler E. The laws governing the fineness of powdered coal. Journal of the Institute of Fuel 1933;7:29–36.
Scott A, McKee DJ. The inter-dependence of mining and mineral beneficiation processes on the performance of mining projects. In: Proceeding of the Australian Institute of Mining and Metallurgy Annual Conference; 1994. p. 5–9.
Segarra Catasús P. Experimental analysis of fragmentation, vibration and rock movement in open pit blasting. PhD Thesis. Universidad Politécnica de Madrid; 2004.
Sereshki F, Hoseini M, Ataei M. Fragmentation measurement using image processing. International Journal of Mining and Geo-Engineering 2016;50(2):211–8.
Si SL, You XY, Liu HC, Zhang P. DEMATEL technique: a systematic review of the state-of-the-art literature on methodologies and applications. Mathematical Problems in Engineering 2018. https://doi.org/10.1155/2018/3696457.
Siddiqui FI, Shah SA, Behan MY. Measurement of size distribution of blasted rock using digital image processing. Journal of King Abdulaziz University: Engineering Sciences 2009;20(2):81–93.
Singh SP, Narendrula R. Causes, implications and control of oversize during blasting. In: Proceedings of the 9th International Symposium on Rock Fragmentation by Blasting; 2009. p. 13–7.
Smith ML, Prisbrey KA, Barron CL. Blasting design for increased SAG mill productivity. Transactions-Society of Mining Engineers of AIME 1994;10(4):188–90.
Sudhakar J, Adhikari GR, Gupta RN. Comparison of fragmentation measurements by photographic and image analysis techniques. Rock Mechanics and Rock Engineering 2006;39(2):159–68.
Thornton DM, Kanchibotla SS, Esterle JS. A fragmentation model to estimate ROM size distribution of soft rock types. In: Proceedings of the 27th Annual Conference on Explosives and Blasting Technique. International Society of Explosives Engineers; 2001. p. 41–53.
Thurley MJ. Automated online measurement of limestone particle size distributions using 3D range data. Journal of Process Control 2011;21(2):254–62.
Tiryaki B. Application of artificial neural networks for predicting the cuttability of rocks by drag tools. Tunnelling and Underground Space Technology 2008;23(3):273–80.
Weisberg S. Applied linear regression, Vol.528. John Wiley and Sons; 2005.

Mohammad Babaeian obtained his BSc degree in Mining Engineering from University of Sistan and Baluchestan, Iran, in 2015 and his MSc degree in Mining Engineering from Shahrood University of Technology, Iran, in 2018. He conducted his thesis about optimization of rock fragmentation to reduce Mine to Mill (M2M) costs in open pit mines. He is the author and co-author of several scientific papers, published in Iranian national journals and international conference proceedings. His research interests include (1) optimization of M2M process, (2) open pit mine design and planning, and (3) size distribution curve analysis of rock mass fragmentation using image processing software, RES and DEMATEL approach. He has been a team member in Jajarm Bauxite Mine Project – (M2M) from 2017 to present.